A Voltage-Zone Based Power Management Scheme With Seamless Power Transfer Between PV-Battery for OFF-Grid Stand-Alone System

Sachin Jain, *Senior Member, IEEE*, Sumon Dhara, *Student Member, IEEE*, and Vivek Agarwal, *Fellow, IEEE*

***Abstract*—There is a requirement for a simple solution that provides seamless power management control and eliminates the issue of toggling between different operating modes in the stand-alone photovoltaic (PV) battery based hybrid system. The solution for the same is given in this article that uses a simple voltage control strategy. The given solution uses a voltage band technique for eliminating the toggling between charging and discharging modes. Further, the toggling between intermediate PV mode with charging and discharging mode is eliminated using the inner voltage band. Thus, the proposed control strategy provides a smooth and seamless control between different modes based on load voltage information. It avoids the overlap of charging and discharging modes within the switching cycle to improve the life-span of the battery. Also, the given control strategy does not require the power information and complex computations like division, etc., for its operation. The given solution can be easily implemented on any PV-battery-based hybrid system having independent control for charging and discharging of the battery with maximum power point tracking (MPPT). A simulation was done to verify the operation in various modes using seamless control. The simulation results are further justified with experimental results from the developed lab prototype.**

***Index Terms*—Battery charging-discharging, efficient power management, photovoltaic (PV) standalone system.**

I. Introduction

ACCORDING to the "State of Electricity Access Report (SEAR) 2017" [1], more than one billion people in various rural and remote areas across the globe still do not have the access to electricity. For this most of the countries across the world have taken several initiatives towards the electrification of all the rural and remote areas [2], [3] by the year 2030. OFF-grid or stand-alone solutions seem to be the best options for the electrification, as it eliminates the requirement of connection with utility apart from transmission and distribution systems requirements [4], [5]. Further, they support distributed generation. Thus, the solutions using pollution-free renewable distributed sources, such assolar photovoltaic, wind, fuel cell, etc., are promoted for the sustainable development of the society. Among all OFF-grid solutions solar photovoltaic (SPV) standalone system is considered to be a good solution due to its ubiquity and sustainability. However, it suffers from the issue of intermittent output in the varying atmosphere. The issue of intermittency can be potentially addressed either by interconnecting complementary energy sources such as wind or natural gas or compiling an energy storage system, such as a battery, super-capacitor [6]–[10]. These energy storage systems play a vital role mainly in the OFF-grid application. The technological advances and rapidly declining prices of both SPV panels and energy storage batteries are making them a more viable solution for the standalone systems for rural electrification. However, the most self-contained and cost-effective approach is to compile the battery [11]–[13] as an energy storage device to meet the PV generation with the load. To balance the load power requirement from the available power in SPV and battery, various power circuit configurations and approaches are given in the literature [14]–[28].

To interface PV, battery, and load, different types of power electronic converters (PEC) are used. Based on the application and voltage conversion ratio, the PEC is chosen accordingly. In the typical solar photovoltaic hybrid system (SPVHS), the bidirectional power converter connects the dc-link with the battery. The bidirectional power converter exchanges the power between dc-link and battery storage as presented in [14]–[16]. The block-diagram of such systems is presented in Fig. 1(a). The given system suffers from the requirement of complex control for seamless power transfer between the sources [17], [18]. Apart from this, the PV power always faces two power conversion stages [stages A and B as shown in Fig. 1(a)] for the battery charging process. Therefore, in order to optimize the power losses in the power conversion stages, a parallel structure of power processing would be an elegant solution as presented in

Manuscript received January 9, 2020; revised July 31, 2020; accepted September 29, 2020. Date of publication October 15, 2020; date of current version December 31, 2020. Paper 2019-SECSC-1485.R1, presented at the 8th IEEE India International Conference on Power Electronics, Jaipur, India, Dec. 13–15, and approved for publication in the IEEE TRANSACTIONS ON INDUSTRY APPLICATIONS by the Renewable and Sustainable Energy Conversion Systems Committee of the IEEE Industry Applications Society. This work was supported in part by the Department of Science and Technology, Govt. of India under the project Optimized and Efficient Stand-Alone PV System for Rural Applications, under Grant DST/TM/SERI/DSS/333(G) dated 20/11/2015. This paper was presented in part at the 8th IEEE India International Conference on Power Electronics Conference, Malaviya National Institute of Technology Jaipur, Jaipur, India, December 2018. *(Corresponding author: Sachin Jain.)*

Sachin Jain is with the Department of Electrical Engineering, National Institute of Technology, Raipur 492010, India (e-mail: sjain.ee@nitrr.ac.in).

Sumon Dhara is with the Department of Electrical Engineering, National Institute of Technology, Warangal 506004, India (e-mail: dsumon@student.nitw.ac.in).

Vivek Agarwal is with the Department of Electrical Engineering, Indian Institute of Technology Bombay, Mumbai 400076, India (e-mail: agarwal@ee.iitb.ac.in).

Color versions of one or more of the figures in this article are available online at https://ieeexplore.ieee.org.

Digital Object Identifier 10.1109/TIA.2020.3031265

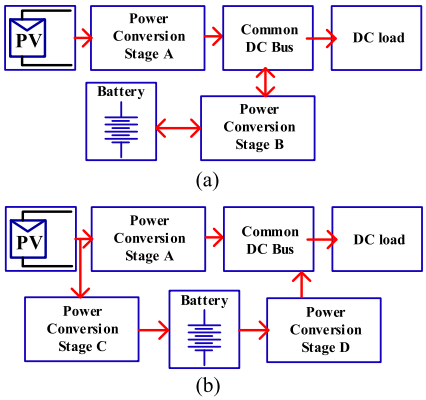

Fig. 1. Block diagram of (a) conventional power processing and (b) proposed structure of power processing stages for PV-battery-based standalone system.

Fig. 1(b), where PV to battery charging is also employed using a single power conversion stage.

Another important solution using the multiport concept is given in the literature [19], [20]. In the given solutions authors have used a three-port converter. The given solution is good, as it possesses the advantages of the low voltage stress across the active switches, reduced number of semiconductor devices. However, these architectures suffer from complex and dependent control loop of the system and no strategy is given for the seamless power flow/control between the sources. Further, to improve the life of the battery simultaneous charging and discharging of the battery within the switching cycle should be avoided. It is also difficult to instantaneously adapt to the transitions among various modes of operation in the given systems. Apart from the converter configurations, many control strategies are also given in the literature.

Now, in [21], a power management strategy using passivity-based control is proposed. The proposed system gives detail with respect to controlling the PV power based on maximum power point tracking (MPPT) and battery state-of-charge (SOC). However, still, the simple scheme for seamless control of the power between SPV and battery is required as the integration of the MPPT with SOC can be added in the system. Another, concept of adding battery connected directly across the load in the dc-link is given in the literature [22], [25]. The PV array output power in such system is usually controlled to maintain the battery SOC within the predefined limits using complex computation control technique, such as sliding mode control, etc. As a consequence, the dc–dc converter will not be controlled to track the maximum power point (MPP) all the time. Further, the basic control scheme does not support the seamless power management. It also does not eliminate the drawback of the toggle between charging and discharging mode when the system operates near the boundary. Moreover, the large surge currents may potentially damage the battery during sudden large load changes due to the absence of the PEC between the battery and the dc bus link. Thus, PEC is necessary for the battery to get connected to the system. Another good approach using a typical PI linear controller is given in the literature [23], [24]. One uses both voltage and power information for the control with ultracapacitor [23]. While the other uses droop control to manage the power balance in the system. Both the solutions use a bidirectional converter with simultaneous charging–discharging mode. However, still, the given control strategy does not provide the seamless control of the power between the sources.

Another good and efficient solution with PV source in the dc-link is given by Akeyo *et al.* [26]. The usage of PV source in the dc link in the system increases its voltage rating requirement. The given solution uses power computations at the input and output, which increases the sensor requirement. Also, the usage of PV source in the dc-link increases the risk of back-feed power. Another novel single-stage transformer-less hybrid system having the feature of boosting, inversion, etc., is given by Alhuwaishel and Enjeti [27]. However, this system uses more passive components and switching devices leading to increased cost and lower reliability. The system given in [27] also suffers from the same drawback of more number of sensors, toggling between various modes, etc. Thus, there is a requirement of seamless control between various modes of operation.

A good solution for SPVHS is proposed by Dhara *et al.* [28]. The given solution processes PV power optimally in a single–stage. The battery charging and discharging modes are decoupled as two separate power converters are employed for each operation. The manuscript gives the detail of the modes of the operation. However, the details with respect to the control strategy and the design of the passive components are not given in the article. The complete detail of the control strategy with supporting experimental and simulation results is given in this article. The proposed system processes the PV and battery power optimally using single-stage power conditioning and avoids the simultaneous charging and discharging of the battery within the switching cycle. Apart from this, a control scheme has been proposed which provides seamless control of power flow between the PV and the battery source. The given control scheme manages the power flow using the information of dc-link or output load voltage. It does not require the information on the PV power for defining the mode of the operation. Further, the given control scheme eliminates the toggle between various modes. Or it discriminates the required operating mode and avoids the overlap to two modes. Thus, during battery charging mode, its overlap with battery discharging mode is eliminated. The same is true for other modes as discussed in the article.

The rest of the article is divided into five sections. Section II gives the details of the proposed system and its various modes of operation. Section III describes the control strategy and the design of the system. Sections IV and V describe the simulation and experimental results of the proposed system respectively. The conclusion of the article is discussed in Section VI.

II. Working Principle and Modes of Operation

The proposed system consists of three basic dc–dc converters, i.e., boost converter, buck converter, and full-bridge converter as shown in Fig. 2. The given system is a good solution for the stand-alone load where the grid is not present. Thus, in

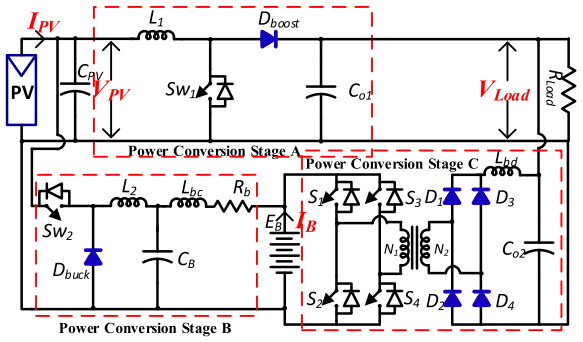

Fig. 2. Circuit schematic for the proposed PV battery fed stand-alone systems.

the proposed system, solar PV is the only source of power generation. Therefore, it becomes important to utilize PV power efficiently and effectively. This can be achieved by operating the PV source near MPP and using single-stage power conditioning for the PV power. Further, the uncertainty of the PV power is taken care by the battery storage. Battery stores the excess power when load requirement is less and supplies the deficit power when available power from PV source is less to meet the load requirement. Thus, the power obtained from the PV source is shared between load and battery. To operate the PV source near MPPT a boost converter is utilized between the PV source and the load. To divert the excess PV power into the battery, a buck converter is employed between them as shown in Fig. 2. Thus, the generated PV power is conditioned in a single-stage whether feeding to load or battery. This helps in the effective utilization of the PV source power.

The proposed configuration is primarily designed to extract maximum power from the PV source. A P&O-based MPPT algorithm is used which operates the PV source near MPP. The maximum power extracted from the PV source is shared by both load and the battery. The output load voltage $V_{\rm Load}$ defines the operation of the buck and full-bridge converter for the charging or discharging of the battery respectively. The output voltage $V_{\rm Load}$ is maintained between the required voltage using PV and battery power. The battery power is used to maintain the $V_{\rm Load}$ during low or zero insolation. So, the battery supplies only the deficient power required by the load to maintain the required $V_{\rm Load}$. On the other hand, if excess power is generated in the PV source, after meeting the load requirement. It is conditioned and diverted for charging of the battery, where electrical energy can be stored for its future use.

From the above-mentioned description, the operation of the proposed system can be classified into the following four modes as given in Table I.

1) Mode I: PV MPPT mode with battery charging.
2) Mode II: PV MPPT mode.
3) Mode III: PV MPPT mode with battery discharging.
4) Mode IV: Battery mode.

Details of the different modes of operation for the proposed configuration with its control scheme using the set reference voltage are as follows.

Mode I: In this mode of operation, PV source is operating at MPP, and the extracted power is utilized to maintain the required

TABLE I
MODES OF OPERATION

Mode	Applicable Condition	Active Source	Active Converter
I	P_{PV}= P_B+P_{req}	PV source and Battery Charging	Boost converter and buck converter
II	P_{PV}= P_{req}	PV source	Boost Converter
III	P_{PV} + P_B = P_{req}	PV source and battery discharging.	Boost converter and Full bridge converter
IV	P_B = P_{req}	Battery Discharging	Full bridge converter

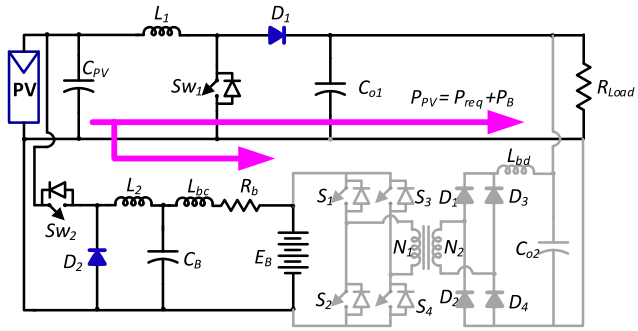

Fig. 3. Equivalent circuit for the mode I operation.

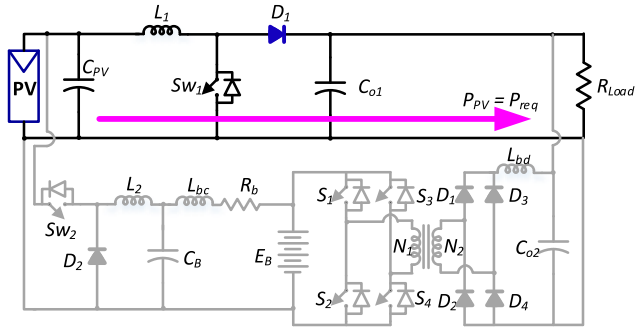

Fig. 4. Equivalent circuit for the mode II operation.

output voltage $V_{\rm Load}$ within the voltage band, apart from battery charging. The same is depicted in Fig. 3 which shows the process of power utilization with active converters. The power extracted from the PV source is conditioned by both boost and buck converters. Boost converter feds the required PV power into the load and the buck converter diverts the excess PV power into the battery as shown in Fig. 3. The duty cycle of the boost is defined by the P&O MPPT algorithm. Buck converter which is controlled by the output voltage $V_{\rm Load}$, diverts the excess PV power into the battery. The buck converter connected at the terminals of the PV source. It directly conditions the excess PV power to be fed into the battery.

Mode II: In this mode of operation (see Fig. 4), there is no excess PV power. The PV power is capable of meeting the load requirement and maintains the required output voltage within the voltage band. So, the only boost converter is active during this mode. It operates the PV source at MPPT and extracts the maximum possible power from the PV source and delivers it to the load as shown in Fig. 4.

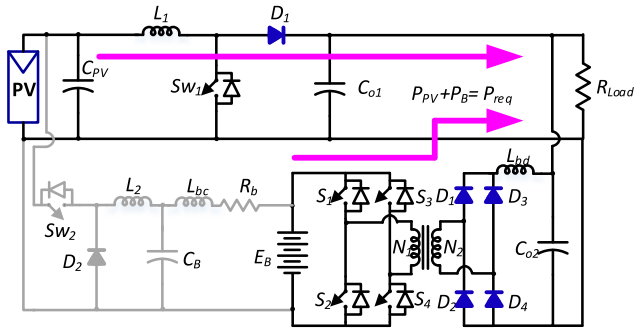

Fig. 5. Equivalent circuit for the mode III operation.

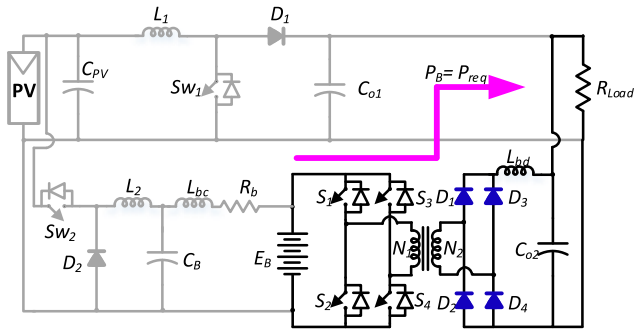

Fig. 6. Equivalent circuit for the mode IV operation.

Mode III: This mode comes into action when the PV power is not sufficient to meet the load demand. During this mode, both the PV source and battery are operated to meet the power requirement of the load. Thus, the deficiency of the power requirement is fulfilled by the battery. So, in this mode of operation, both boost converter and the full-bridge converter are active converters as shown in Fig. 5. Boost converter extracts maximum available power from PV. The rest of the required power is met by a battery using a full-bridge converter.

Mode IV: In this mode of operation (see Fig. 6), the generated power in the PV source is not significant or nearly zero, due to the absence of the sunlight or near to zero insolation level. So, battery stored power is utilized to meet the required load demand. Thus, the full-bridge converter processes the battery power and meets the load requirement and maintains the dc-link voltage at $V_{\mathrm{DC(ref\,Low)}}$ volts as shown in Fig. 6.

III. Control Strategy

The proposed system has four modes of operation. In modes I, II, and III the system operates the PV source near or at MPPT. It is done by the dedicated boost converter with its MPPT controller. As the MPPT control works independently, so any of the MPPT algorithms such as the P&O algorithm, Hill Climbing, incremental conductance algorithm, RCC algorithm, beta algorithm [29], etc., can be employed in this control scheme. However, to simplify the overall scheme, the conventional P&O algorithm is employed as shown in Fig. 7(b). The P&O MPPT algorithm uses the slope information of the *P–V* curve using PV voltage and current information for generating the reference

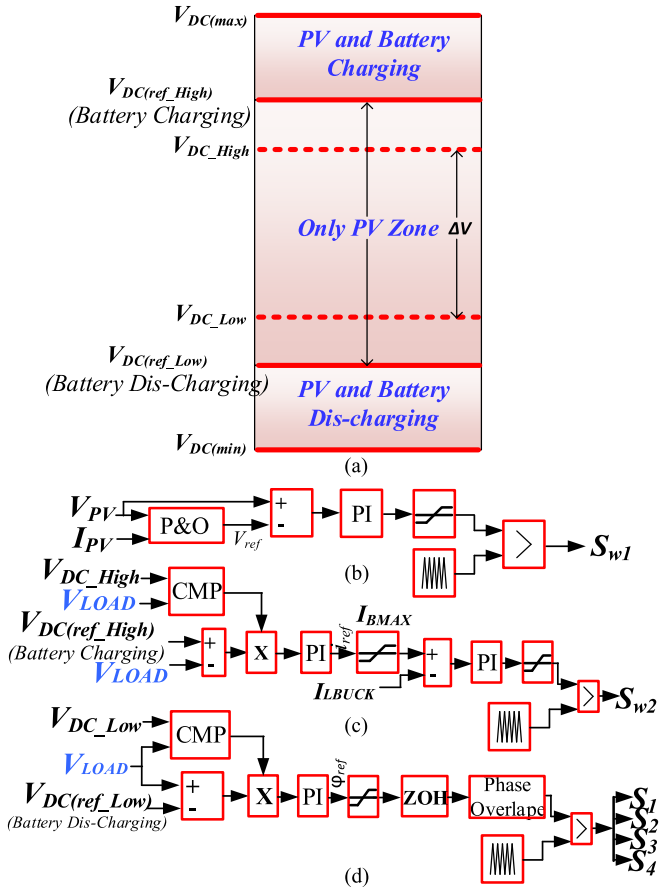

Fig. 7. (a) Voltage bands for seamless mode transition. (b) Control block diagram for the MPPT algorithm implementation. (c) Control block diagram for battery charging controller. (d) Control block diagram for battery discharging controller.

PV voltage signal as an output. The reference output voltage signal is then compared with the actual PV voltage to generate the voltage error, which again is given to the PI controller for the generation of the duty cycle for the boost converter.

Apart from boost converter system has buck and full-bridge converter dedicated for battery charging and discharging, respectively, as discussed in the above section describing different modes of the operation. It required that system should move from one mode to another seamlessly. For this, it is required that the system should not toggle between its four operating modes. In other words, if the system operates in mode-I, it should not toggle between modes (I or II) or modes (II and III). When the system moves from modes I to III, it should first move to mode II and then to mode III. In other words, when the operation of the system in battery charging (mode I) moves to battery discharging mode (mode III) by passing through mode II in which the only PV is trying to meet the load demand. The same is true for vice-versa, i.e., when the system moves from modes III to I. This is attained with the help of the voltage band (ΔV) as given in Fig. 7. The voltage band ΔV is the difference of the activation voltages for discharging mode ($V_{\mathrm{DC\_Low}}$) from the charging mode ($V_{\mathrm{DC\,High}}$) as given in Fig. 7. This avoids the overlap of the charging and discharging mode. The difference between the

set voltages discriminates between modes I and III and avoids toggling between them.

Further to avoid the toggling between modes I and mode II (especially when the system moves from modes I to II or vice versa), a simple trick is employed by setting the reference voltage $V_{\mathrm{DC(ref\,High)}}$ used for generating the control signal for the buck converter is higher than the charging activation voltage $V_{\mathrm{DC\_High}}$. This can be seen in the control loop diagram for the buck converter shown in Fig. 7. This not only avoids the toggle between two modes but also helps in seamless transfer from one mode to another. Similar approach has been used to avoid toggle between modes II and III. The set reference voltage $V_{\mathrm{DC(ref\,Low)}}$ for the discharging of the battery via a full-bridge converter is set lower than the $V_{\mathrm{DC\_Low}}$. This can be seen in the control loop diagram for the full-bridge converter shown in Fig. 7. Therefore, although the activation signal for discharging full-bridge converter is active, still the converter will not be turned-ON, till the output voltage falls below the reference voltage $V_{\mathrm{DC(ref\,Low)}}$. Thus, the system comes to mode III after passing through mode II or vice-versa. Also, it avoids the toggle between modes III and II, when the system moves from modes III to II or vice versa. This can be supported by the fact that when the system moves from modes III to II, its output voltage lies between $V_{\mathrm{DC(ref\,Low)}}$ and $V_{\mathrm{DC\_Low}}$, where the duty cycle for the full-bridge converter is negative or zero. In other words, the voltage error is negative which makes the duty cycle of the full-bridge converter to reduce to zero. Thus, the system operates seamlessly between modes II and III.

IV. Design of Proposed SPVHS

A. Boost Converter Design for MPPT

The design perspective of the boost stage of the proposed configuration follows the conventional design of a boost converter [30], [31]. There are various types of algorithms to track the MPP using power converters. The power converter operates the PV source near MPP using the voltage or duty cycle control governed by the MPPT algorithm. Typically, power converters manipulate the output resistance seen by the PV source with the help of the MPP algorithm and bring it close to the MPP resistance R_{mpp}. The MPP resistance R_{mpp} is the total resistance is required to be seen by the source to achieve MPP condition. It can also be calculated as

$$R_{\mathrm{mpp}} = \frac{V_{\mathrm{mpp}}}{I_{\mathrm{mpp}}}. \tag{1}$$

Now, assuming the system is ideal with the input power equal to the output power, assuming continuous conduction mode for boost converter, the following equation can be derived as:

$$P_{\mathrm{in}} = P_{\mathrm{out}} = \frac{V_{\mathrm{mpp}}^2}{R_{\mathrm{mpp}}} = \frac{V_{\mathrm{Load}}^2}{R_{\mathrm{Load}}} = \frac{V_{\mathrm{mpp}}^2}{(1-D_{\mathrm{mppt}})^2 R_{\mathrm{Load}}}. \tag{2}$$

The R_{Load} (i.e., load resistance) is required to be estimated with respect to the required output power at a constant output voltage (V_{Load}) of $V_{\mathrm{DC(ref\,High)}}$. Therefore, with respect to the maximum and minimum irradiance corresponding, $D_{\max}$ and $D_{\min}$ can be obtained from the above equation. The inductance of the boost converter (L_1) can be designed for minimum irradiance ($D_{\mathrm{mppt}} = D_{\min}$) as per the following equation:

$$L_1 = \frac{V_{\mathrm{mpp}} D_{\mathrm{mppt}}}{\Delta i_L f_{\mathrm{sw}}} \tag{3}$$

where Δi_L is the inductor current ripple and f_{sw} is the switching frequency of the boost converter. The input capacitor of the boost converter can be designed from the following equation considering the allowable voltage ripple across the PV module terminal (ΔV_{mpp}) for maximum insolation ($D_{\mathrm{mppt}} = D_{\max}$):

$$C_{\mathrm{PV}} = \frac{D_{\mathrm{mppt}}}{8 L_1 \Delta V_{\mathrm{mpp}} f_{\mathrm{sw}}^2} \tag{4}$$

The output capacitance of the boost converter is determined using the following equation for maximum insolation ($D_{\mathrm{mppt}} = D_{\max}$), and allowable output voltage ripple (ΔV_{Load})

$$C_{o1} = \frac{D_{\mathrm{mppt}} V_{\mathrm{Load}}}{R_o \Delta V_{\mathrm{Load}} f_{\mathrm{sw}}}. \tag{5}$$

B. Buck Converter Design for Battery Charging

The design of the buck-stage of the proposed configuration is extended from the design procedures given in [32]. The components of the buck converter are chosen using the criteria of maximum allowable battery charging current (I_{BMAX}), the MPP voltage of the PV module, and the battery voltage (E_B). The duty cycle (d_{charging}) of the buck converter can be determined by the following equation:

$$d_{\mathrm{charging}} = \frac{V_B}{V_{\mathrm{mpp}}}. \tag{6}$$

Similarly, the inductor (L_2) for the buck converter can be designed based on the maximum allowable ripple current (ΔI_B) and the input PV voltage and the battery voltage as given in the following equation:

$$\mathrm{L_2} = \frac{E_B(V_{\mathrm{mpp}} - E_B)}{\Delta I_B}. \tag{7}$$

In order to maintain a stiff output voltage to charge the battery with reduced ripple content, the capacitor at the output of the buck-converter can be chosen as per the following equation:

$$\mathrm{C_B} = \frac{\Delta I_B}{8 f_{\mathrm{sw}} \Delta V_B} \tag{8}$$

where ΔV_B is the voltage ripple across the output side capacitor of the buck converter C_B.

C. Full-Bridge Converter Design for Battery Discharging

In order to achieve a high-voltage gain, a phase-shifted full-bridge converter is employed between the battery and dc link. The phase-overlap between the two-leg of full-bridge converter gives the effective active powering duration for the full-bridge converter. The active power transfer duration can be derived from the literature [33], [34] as per the following equation:

$$d_{\mathrm{discharging}} = 0.5\left(\frac{V_{\mathrm{Load}}}{V_B}\right)\left(\frac{N_1}{N_2}\right) = 0.5\left(\frac{V_{\mathrm{Load}}}{nV_B}\right) \tag{9}$$

TABLE II
PARAMETERS USED FOR SIMULATION

1.	PV open-circuit voltage (V_{OC})	190V
2.	PV Capacitance C_{PV}	1mF
3.	Load Capacitor (C_{o1}, C_{o2})	100uF
4.	Load Resistance (R_{Load})	800Ω
5.	Boost Inductor (L_1)	1.5mH
6.	Buck Inductor (L_2)	1mH
7.	Battery charging inductor (L_{bc})	10uH
8.	Battery Voltage (E_b)	48V
9.	High-frequency Transformer (N_1:N_2)	1:8
10.	Battery dis-charging Inductor (L_{bd})	2mH
11.	Switching frequency (f_{sw})	20kHz

$$n = \frac{N_2}{N_1} \tag{10}$$

where N_1, N_2, and $d_{\text{discharging}}$ represent the primary and secondary turn ratio of the full-bridge transformer, active duty cycle of the converter, respectively. The magnetizing inductance L_{mag} of the transformer can be derived as per the following equation:

$$L_{\text{mag}} = \frac{V_B(1 - d_{\text{discharging}})}{0.5\Delta I_L f_{\text{sw}}}. \tag{11}$$

Now, the filter inductor and capacitor of the full-bridge converter to eliminate the switching ripple harmonics can be designed from the following equation:

$$L_{bd} = \frac{(nV_B - V_{\text{Load}})d_{\text{discharging}}}{\Delta I_L f_{\text{sw}}} \tag{12}$$

$$C_{\text{o2}} = \frac{d_{\text{discharging}}\Delta I_L}{\Delta V_o f_{\text{sw}}}. \tag{13}$$

From the above given equations, the passive components of the proposed converter are chosen. The closed-loop control for the proposed system is implemented and analyzed using Powersim (i.e. PSIM Electronic Simulation Software) (PSIM), The values k_p (proportional gain) and k_i (integral gain) of the PI controllers are obtained using the smart-control-tool of PSIM and is used in the simulation and experimental setup.

V. SIMULATION RESULT

The proposed PV-Battery based standalone configuration, along with its control strategy, is simulated in the PSIM environment. PV and battery sources are realized in the PSIM function blocks with the help of their modeling equations. The simulation is done with variable insolation conditions to justify its four modes of operation and control methodology. The parameters used in the simulation are given in Table II.

In the simulation environment, the MPPT controller is triggered at 0.05s, and thereafter at 0.15s, the battery controller is triggered. The delay is introduced to facilitate the system to prioritize the MPPT control rather than battery control, during the initial start of the system. Fig. 8 shows the simulation results for four modes of operation, while the insolation is varied in steps as shown in Fig. 8(a). Subplots (b) and (c) of Fig. 8 show the operating PV voltage (V_{PV}) with the MPPT voltage reference (V_{PV}) and PV current (I_{PV}), respectively. The PV voltage follows the MPPT reference voltage. Tracking of the

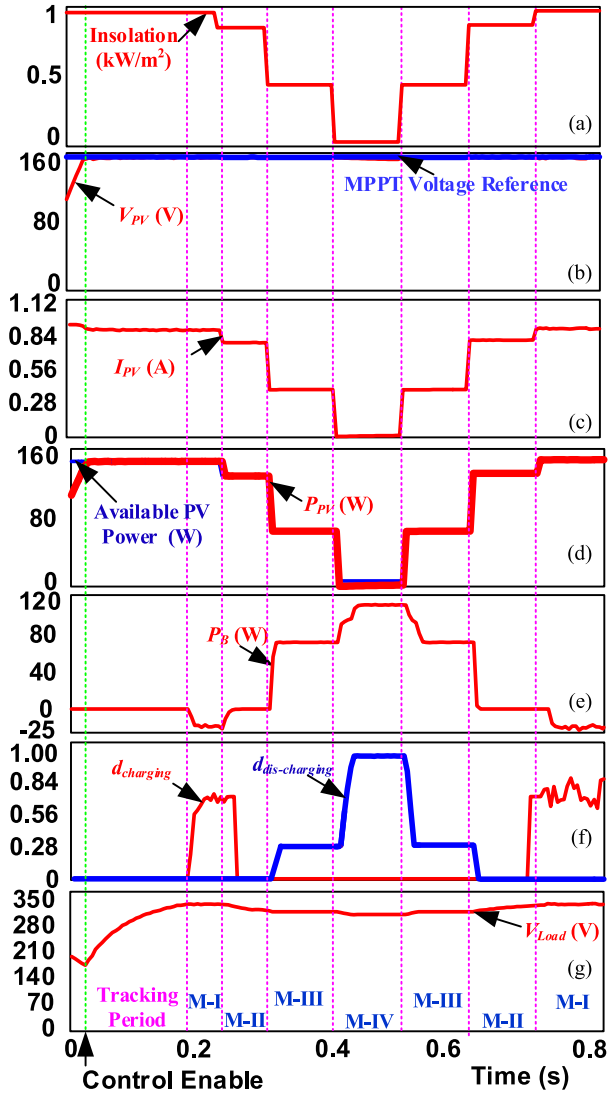

Fig. 8. Simulated performance of the system. (a) Change in insolation. (b) MPPT reference. (c) PV source current (I_{PV}). (d) PV power output (P_{PV}). (e) Battery power(P_B). (f) Charging and discharging duty reference (d_{charging}, $d_{\text{discharging}}$). (g) Load voltage (V_{Load}) when the insolation of the PV source is varied in small steps from maximum to minimum and increased from minimum to maximum.

MPP power can be observed from subplot (d) which shows actual available and tracked PV power. The other subplots (e)–(g) in Fig. 8 show the battery power, battery converter control reference and output voltage (V_{Load}), respectively. The decrease or increase of PV MPP power results in an increase and decrease of the battery discharging power, which can be observed in subplot (e) of Fig. 8. Further, the battery power is negative, when it is getting charged by the PV power (i.e., mode I charging mode) and is positive when getting discharged. Further, there is no overlap between the charging (mode I) and discharging (modes III and IV) modes of the battery. This is also supported by the battery charging and discharging duty reference waveforms given in the subplot (f) of Fig. 8. Further, there exists mode II between charging and discharging modes, when PV power matches the load requirement. The operation

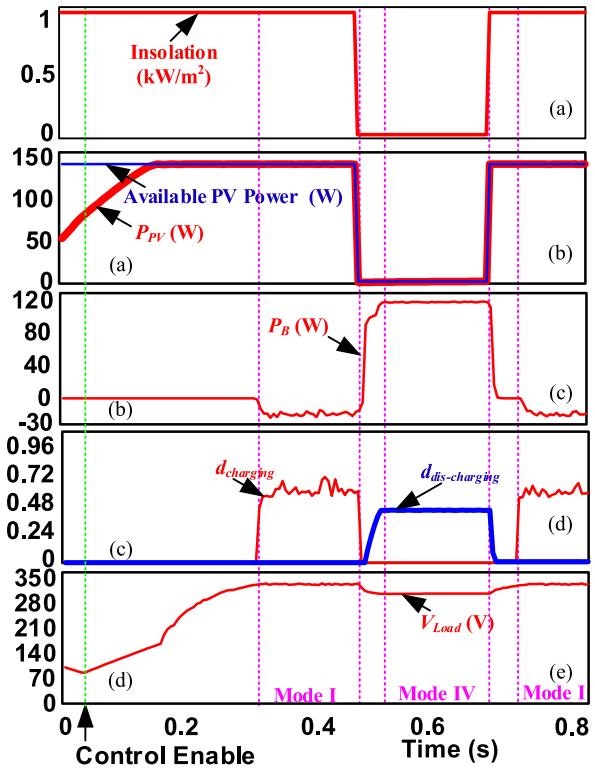

Fig. 9. Simulated performance of the system. (a) Change in insolation. (b) PV power output (P_{PV}). (c) Battery power (P_B). (d) Charging and discharging duty reference (d_{charging}, $d_{\mathrm{discharging}}$). (e) Output voltage (V_{Load}) when the insolation of the PV Source changed in step from maximum to minimum and minimum to maximum.

of the system in mode II can be observed between charging and discharging modes, thus eliminating the chances of overlap between them. This also improves the life-span of the battery by eliminating the unwanted charging and discharging cycle of the battery. The charging and discharging duty reference control signals have zero value during mode II. While during battery charging or discharging modes their corresponding charging and discharging duty reference control signals are positive and otherwise have zero value. This supports the seamless mode transfer of the system. Also, the considered voltage band in control can be observed in the output voltage waveform shown in the subplot (g) of Fig. 8.

Further to justify the nonoverlap of the different modes a worst case has been simulated, where the system moves from modes I to IV and back to mode I as shown in Fig. 9. The step-change in the insolation from maximum to minimum and minimum to maximum is shown in Fig. 9(a). The smooth transition from modes I to IV can be verified with the charging and discharging duty reference control signals as shown in the subplot (d) of Fig. 9. The charging and discharging duty reference control signal waveforms are not having any overlap between them. As the PV power is reduced to zero instantaneously, so the system moves from modes I to IV while passing through modes II and III. Further, when PV power retrieves with an initial value of mode I, the system smoothly transfers to mode I, while passing through modes III and II in sequence. This can be observed

TABLE III
COMPARISON OF EFFICIENCY

Mode	Applicable Condition	$\eta_{Proposed}$	$\eta_{overall}$
I	$P_{PV}= P_B+P_{req}$	η_{PVL} =97.9% η_{PVB} =93.9%	η_{OL} = 95.9%
II	$P_{PV}= P_{req}$	η_{PVL} =97.7%	η_{OL} =97.7%
III	$P_{PV} + P_B = P_{req}$	η_{PVL} =97.9% η_{BL} =92.2%	η_{OL} = 95%
IV	$P_B = P_{req}$	η_{BL} =92.0%	η_{OL} =92.0%

p_{al} = power conversion efficiency for PV source to load, p_{ub} = power conversion efficiency for PV source to battery charging η_{BL} = power conversion efficiency for the battery to load, and η_{OL} = overall efficiency in a particular mode of operation.

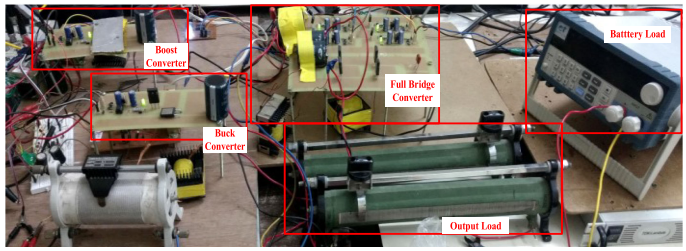

Fig. 10. Experimental prototype for the proposed system.

from the waveform of charging and discharging duty reference control signals, apart from battery power. The decreasing battery power and value of discharging duty reference control signal with PV source operating at MPP supports mode III. The zero value of both charging and discharging duty reference control signals justifies the mode II operation of the system. Thus, the given control strategy takes care of the seamless transfer between various modes.

Now, in order to quantify the performance of the proposed system during various operating modes, extensive loss analysis was performed using simulations on PLECS software platform. In the simulations, power switch and diode with part numbers SPW47N60C3 (Cool MOS Power Transistor) and DPH30IS600HI, respectively, are considered for power loss calculation. The analysis is done for the 1kW system with the same voltage levels (as considered in the simulation analysis). Thus, a 1kW PV panel with the required output is simulated to analyze losses in four operating modes of the system. Table III summarizes the comprehensive list of the efficiency of the system for each mode of operation. It is observed that during PV to battery charging in mode I, a relative increment of 4% efficiency can be achieved using the proposed SPVHS as compared with the conventional solutions [14]–[16].

VI. EXPERIMENTAL RESULTS

To support the simulation results an experimental prototype of the proposed system is developed with a power capacity of 200 Watt. The experimental prototype consists of two programmable dc sources, an electronic load, a resistive load, and the required converters as shown in Fig. 10. The parameters used for the experimental prototype are given in Table IV. The fabricated converters were developed using 47N60C3 and DPH30IS600HI

TABLE IV
PARAMETERS USED FOR EXPERIMENTAL PROTOTYPE

1.	PV open-circuit voltage (V_{OC})	65V
2.	PV short circuit current (Isc)	0.95A
3.	PV Capacitance C_{PV}	1mF
4.	Load Capacitor (C_{o1}, C_{o2})	1mF
5.	Load Resistance (R_{Load})	500Ω
6.	Boost Inductor (L_1)	1.5mH
8.	Buck Inductor (L_2)	800uH
9.	Battery Voltage (E_b)	18V
10.	High-frequency Transformer (N_1: N_2)	1:7
11.	Battery dis-charging Inductor (L_{bd})	1mH
12.	Switching frequency(f_{sw})	20kHz
13.	$V_{DC(max)}$	130V
14.	$V_{DC(ref\ High)}$ (Battery Charging)	120V
15.	$V_{DC\ High}$	115V
16.	$V_{DC\ Low}$	105V
17.	$V_{DC(ref\ Low)}$ (Battery dis-charging)	100V
18.	$V_{DC(min)}$	90V

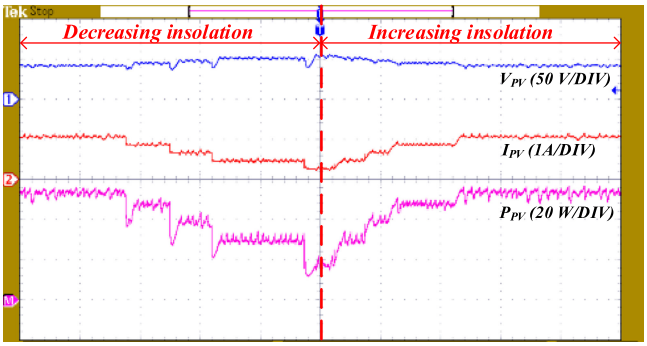

Fig. 11. Experimental results showing the waveforms of the PV voltage, PV current, and PV power at varying insolation conditions (emulated by changing the current references of the dc source).

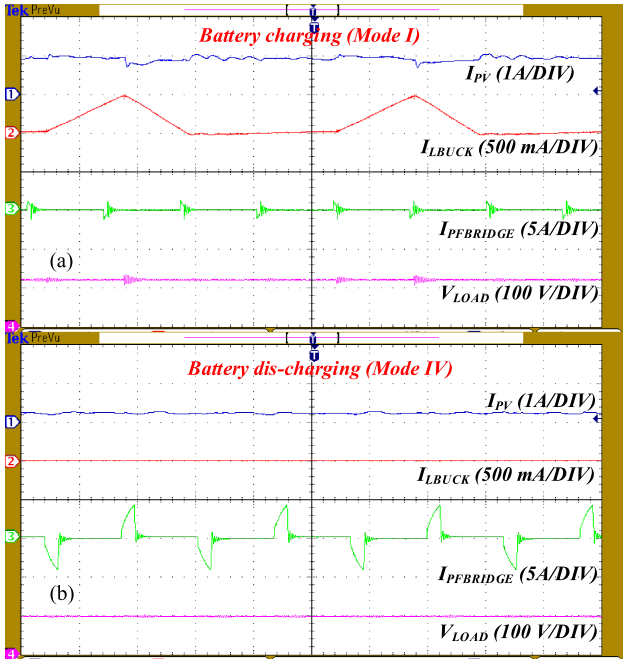

Fig. 12. Experimental results showing the waveforms of the PV current, battery charging current, primary current of full-bridge converter, and load voltage for (a) mode I and (b) mode IV.

power diodes. The control pulses for the converters are generated using Texas Instruments TMDX28069 USB 32-bit floating-point microcontrollers and DSpace 1104 with required necessary signal conditioning and level shifting circuitry.

Using the fabricated set-up various important waveforms to support the operation of the proposed system were captured in the oscilloscope Tektronix MOD 3034 are shown in Figs. 12–15. The PV source is emulated in the experimental set-up using a programmable power supply with a small series resistance [35], [36]. The varying isolation conditions are emulated by changing the current reference value in the programmable dc source. Important waveforms of emulated PV source operating at MPP for (both decreasing isolation conditions are shown in Fig. 11. The MPP tracking by the boost converter can be verified from the PV power waveforms.

The battery acts as a sink or source for the excess or deficit PV power as shown in Fig. 12(a) and (b), respectively. The inductor current I_{LBUCK} of the buck converter and the transformer primary current $I_{PFbridge}$ of the full-bridge converter is responsible for the charging and discharging of the battery respectively. Further, charging and discharging event should not occur simultaneously. This can be justified from Fig. 13, where either battery charging current I_{LBUCK} or battery discharging current ($I_{PFbridge}$) flows in the system.

Also, the higher the output voltage (V_{Load}) in charging mode (mode I) of operation compared to battery discharging mode (mode IV) of operation can be seen in Figs. 13 and 14. This further supports the control strategy and its operation in the proposed system. To justify operation in all the four modes, waveforms were taken from the experimental prototype as shown in Fig. 13(a) and (b). The small variation in the output voltage (V_{Load}) in the given band for different modes supports the control strategy. The operation of the PV source near MPP can be observed from PV power waveform and MPPT duty reference.

Another important thing to be noted is with respect to duty reference for charging (mode I) and discharging (mode IV) operation. It can be observed that the two reference waveforms do have a value of more than zero simultaneously. Thus, only one or none among the two-reference value have value more than zero. This supports the statement that charging and discharging operations do not occur simultaneously. Apart from this seamless control and elimination of the toggle between various modes can be seen from Figs. 13 and 14. The magnitude of the mentioned two waveforms did not become nonzero simultaneously. It can be observed that battery charging duty is nonzero only during mode I whereas, the battery discharging duty is nonzero only during modes III and IV. For the mode II operation, both the references are zero. Apart from these, seamless mode transition control and elimination of toggling between various modes are observed from the waveform presented in Fig. 13. This can be supported by the existence of mode-II (only PV mode), which

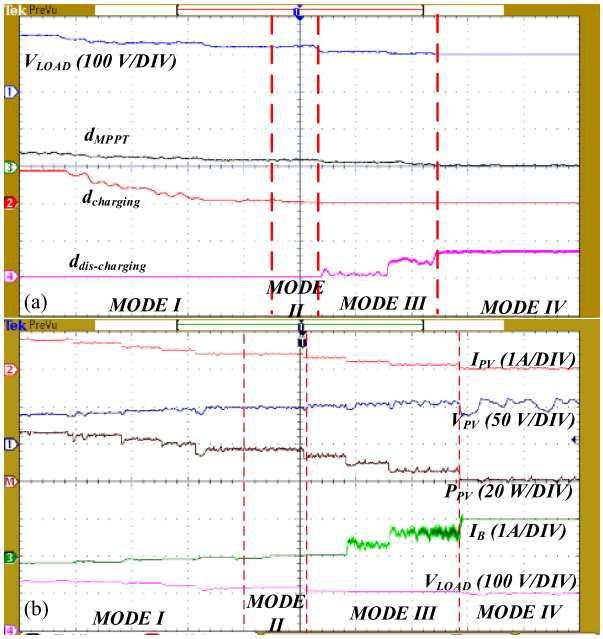

Fig. 13. Experimental results for (a) Load voltage, MPPT duty reference (d_{umpty}), battery charging duty reference (d_{charging}), battery discharging duty reference ($d_{\text{discharging}}$). (b) PV current, PV voltage, PV power, battery current, and output voltage (V_{Load}) to justify the performance of proposed control strategy during step transitions among different modes of operation.

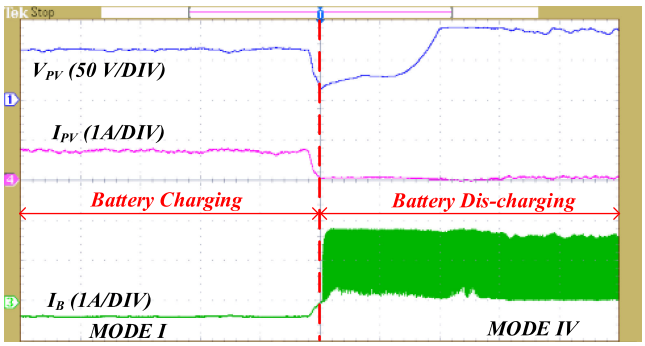

Fig. 14. Experimental results of PV voltage, PV current and battery current during the extreme condition (i.e., direct transition from modes I to IV).

occurs between modes I and III. During this mode value of both charging and di-charging duty-reference is zero. This can also be supported with the transition of battery current from negative to zero and zero to positive as shown in Fig. 13. Further to support the seamless transition in extreme conditions, results are taken from the developed prototype having a step change of PV current from max to zero to push the mode of operation from modes I to IV. The set current reference in the dc source emulating PV array is set to zero from its maximum value to emulate the change of isolation condition. The controller prioritizes the event of reduction of battery charging current to zero and then starts discharging (mode IV) operation as shown in Fig. 14.

VII. Conclusion

In this article, the performance of the proposed simple and seamless control strategy for the PV-battery powered hybrid system was verified using simulations and experimental results. The topology employed for the verification of the control strategy had a dedicated converter for each operation. The employed configuration processed the power whether extracted from PV or battery source in parallel and single-stage operation improved the system performance. Further, the proposed control strategy supports smooth power management between PV, battery, and load. The same was verified in simulation and experimental results. The proposed control strategy avoids toggling between charging and discharging modes by employing a voltage band between them. It also eliminated the toggling of charging and discharging modes with an intermediate PV mode by using another inner voltage band. Thus, the given control scheme avoided the overlap or occurrence of the two modes simultaneously. Furthermore, the elimination of the overlap between charging and discharging modes also extended the life span of the battery. Seamless power control, when the system moved from charging to discharging mode or vice versa, is also verified from simulations and experimental results. Thus, the given control strategy was simple and easy to implement as it is based on output voltage control. It does not require individual power computations and complex computations, such as division, nonlinear iteration, etc. It can be easily applied to any PV hybrid system having independent control for charging, discharging, and the MPPT operation.

References

[1] State of electricity access report 2017, Wikipedia. [Online]. Available: http://documents.worldbank.org/curated/en/364571494517675149/full-report, Accessed on: May 1, 2017.

[2] Y. Mekonnen and A. I. Sarwat, "Renewable energy supported microgrid in rural electrification of sub-Saharan Africa," in *Proc. IEEE PES Power Africa*, 2017, pp. 595–599.

[3] M. Nasir, M. Anees, H. A. Khan, I. Khan, Y. Xu, and J. M. Guerrero, "Integration and decentralized control of standalone solar home systems for off-grid community applications," *IEEE Trans. Ind. Appl.*, vol. 55, no. 6, pp. 7240–7250, Nov./Dec. 2019.

[4] J. Philip *et al.*, "Control and implementation of a standalone solar photovoltaic hybrid system," *IEEE Trans. Ind. Appl.*, vol. 52, no. 4, pp. 3472–3479, Apr. 2016.

[5] M. J. E. Alam, K. M. Muttaqi, and D. Sutanto, "Effective utilization of available PEV battery capacity for mitigation of solar PV impact and grid support with integrated V2G functionality," *IEEE Trans. Smart Grid*, vol. 7, no. 3, pp. 1562–1571, May 2016.

[6] H. Wang and Z. Jiancheng, "Research on charging/discharging control strategy of battery-super capacitor hybrid energy storage system in photovoltaic system," in *Proc. IEEE 8th Int. Power Electron. Motion Control Conf.*, 2016, pp. 2694–2698.

[7] L. Pan, J. Gu, J. Zhu, and T. Qiu, "Integrated control of smoothing power fluctuations and peak shaving in wind/pv/energy storage system," in *Proc. 8th Int. Conf. Intell. Human-Mach. Syst. Cybern.*, 2016, pp. 586–591.

[8] D. B. W. Abeywardana, B. Hredzak, V. G. Agelidis, and G. D. Demetriades, "Supercapacitor sizing method for energy-controlled filter-based hybrid energy storage systems," *IEEE Trans. Power Electron.*, vol. 32, no. 2, pp. 1626–1637, Feb. 2017.

[9] V. I. Herrera, H. Gaztañaga, A. Milo, A. Saez-de-Ibarra, I. Etxeberria-Otadui, and T. Nieva, "Optimal energy management and sizing of a battery–supercapacitor-based light rail vehicle with a multi-objective approach," *IEEE Trans. Ind. Appl.*, vol. 52, no. 4, pp. 3367–3377, Jul./Aug. 2016.

[10] V. F. Pires, D. Foito, and A. Cordeiro, "A DC–DC converter with quadratic gain and bidirectional capability for batteries/supercapacitors," *IEEE Trans. Ind. Appl.*, vol. 54, no. 1, pp. 274–285, Jan./Feb. 2018.

[11] Y. Liu and S. Chen, "Development of a simulation-based electricity analysis environment for a community microgrid system," in *Proc. IEEE Int. Conf. Appl. Syst. Innov.*, 2017, pp. 1461–1464.

[12] F. Cingoz, A. Elrayyah, and Y. Sozer, "Optimized resource management for PV–fuel-cell-based microgrids using load characterizations," *IEEE Trans. Ind. Appl.*, vol. 52, no. 2, pp. 1723–1735, Mar./Apr. 2016.
[13] S. Kumar Tiwari, B. Singh, and P. K. Goel, "Design and control of microgrid fed by renewable energy generating sources," *IEEE Trans. Ind. Appl.*, vol. 54, no. 3, pp. 2041–2050, May/Jun. 2018.
[14] S. Mishra and R. K. Sharma, "Dynamic power management of PV based islanded microgrid using hybrid energy storage," in *Proc. IEEE 6th Int. Conf. Power Syst*., 2016, pp. 1–6.
[15] S. Daher, J. Schmid, and F. L. M. Antunes, "Multilevel inverter topologies for stand-alone PV systems," *IEEE Trans. Ind. Electron.*, vol. 55, no. 7, pp. 2703–2712, Jul. 2008.
[16] S. Malo and R. Grino, "Design, construction, and control of a stand-alone energy-conditioning system for PEM-type fuel cells," *IEEE Trans. Power Electron.*, vol. 25, no. 10, pp. 2496–2506, Oct. 2010.
[17] S. S Nag and S. Mishra, "Current-fed switched inverter," *IEEE Trans. Ind. Electron.*, vol. 61, no. 9, pp. 4680–4690, Sep. 2014.
[18] K. Tseng and C. Huang, "High step-up high efficiency interleaved converter with voltage multiplier module for renewable energy system," *IEEE Trans. Ind. Electron.*, vol. 61, no. 3, pp. 1311–1319, Mar. 2014.
[19] F. Nejabatkhah, S. Danyali, S. H. Hosseini, M. Sabahi, and S. Niapour, "Modeling and control of a new three-input DC–DC boost converter for hybrid PV/FC/Battery power system," *IEEE Trans. Power Electron.*, vol. 27, no. 5, pp. 2309–2323, May 2012.
[20] H. Wu, K. Sun, R. Chen, H. Hu, and Y. Xing, "Full-bridge three port converters with wide input voltage range for renewable power systems," *IEEE Trans. Power Electron.*, vol. 27, no. 9, pp. 3965–3974, Sep. 2012.
[21] A. Tofighi and M. Kalantar, "Power management of PV/battery hybrid power source via passivity-based control," *Renew. Energy*, vol. 36, no. 9, pp. 2440–2450, Sep. 2011.
[22] S. J. Chiang, H. Shieh, and M. Chen, "Modeling and control of PV charger system with SEPIC converter," *IEEE Trans. Ind. Electron.*, vol. 56, no. 11, pp. 4344–4353, Nov. 2009.
[23] H. Fakham, D. Lu, and B. Francois, "Power control design of a battery charger in a hybrid active pv generator for load-following applications," *IEEE Trans. Ind. Electron.*, vol. 58, no. 1, pp. 85–94, Jul. 2011.
[24] H. Mahmood, D. Michaelson, and J. Jiang, "A power management strategy for pv/battery hybrid systems in islanded microgrids," *IEEE J. Emerg. Sel. Topics Power Electron.*, vol. 2, no. 4, pp. 870–882, Jun. 2014.
[25] M. Rezkallah, A. Hamadi, A. Chandra, and B. Singh, "Real-Time HIL implementation of sliding mode control for standalone system based on PV array without using dumpload," *IEEE Trans. Sustain. Energy*, vol. 6, no. 4, pp. 1389–1398, Oct. 2015.
[26] O. Akeyo, V. Rallabandi, N. Jewell, and D. M. Ionel, "Improving the capacity factor and stability of Multi-MW grid connected PV systems with results from a 1MW/2MWh battery demonstrator," in *Proc. IEEE Energy Convers. Congr. Expo*., 2018, pp. 2504–2509.
[27] F. Alhuwaishel and P. Enjeti, "A single stage Transformer-less micro inverter with integrated battery storage system for residential applications," in *Proc. 20th Workshop Control Model. Power Electron*., 2019, pp. 1–7.
[28] S. Dhara, S. Jain, and V. Agarwal, "A novel voltage-zone based power management scheme for PV- Battery based standalone system," in *Proc. IEEE India Int. Conf. Power Electron*., 2018, pp. 1–6.
[29] X. Li, H. Wen, L. Jiang, W. Xiao, Y. Du, and C. Zhao, "An improved MPPT method for PV system with fast-converging speed and zero oscillation," *IEEE Trans. Ind. Appl.*, vol. 52, no. 6, pp. 5051–5064, Nov./Dec. 2016.
[30] A. Razman and C. W. Tan, "Design of boost converter based on maximum power point resistance for photovoltaic applications," *Solar Energy*, vol. 160, pp. 322–335, Jan. 2018.
[31] L. V. Bellinaso, H. H. Figueira, M. F. Basquera, R. P. Vieira, H. A. Gründling, and L. Michels, "Cascade control with adaptive voltage controller applied to photovoltaic boost converters," *IEEE Trans. Ind. Appl.*, vol. 55, no. 2, pp. 1903–1912, Mar./Apr. 2019.
[32] D. Venkatramanan and V. John, "Dynamic modeling and analysis of buck converter based solar PV charge controller for improved MPPT performance," *IEEE Trans. Ind. Appl.*, vol. 55, no. 6, pp. 6234–6246, Nov./Dec. 2019.
[33] "UCC28950 600-W, phase-shifted, full-bridge application report," Texus Instrument Application Report, Jun. 2011, [Online]. Available: http://www.ti.com/lit/an/slua560c/slua560c.pdf
[34] R. Chen, T. Liang, J. Chen, R. Lin, and K. Tseng, "Study and implementation of a current-fed full-bridge boost DC–DC converter with zero-current switching for high-voltage applications," *IEEE Trans. Ind. Appl.*, vol. 44, no. 4, pp. 1218–1226, Jul./Aug. 2008.
[35] S. Jain, R. Karampuri, and V. T. Somasekhar, "An integrated control algorithm for a single-stage PV pumping system using an open-end winding induction motor," *IEEE Trans. Ind. Electron.*, vol. 63, no. 2, pp. 956–965, Feb. 2016.
[36] V. Sonti, S. Jain, and S. Bhattacharya, "Analysis of the modulation strategy for the minimization of the leakage current in the PV grid-connected cascaded multilevel inverter," *IEEE Trans. Power Electron.*, vol. 32, no. 2, pp. 1156–1169, Feb. 2017.

Sachin Jain (Senior Member, IEEE) received the B.E degree in electrical engineering from the Bhilai Institute of Technology, Bhilai, India, in 2000, the M.Tech degree in integrated power systems from the Visvesvaraya National Institute of Technology, Nagpur, India, in 2002, and the Ph.D. degree from the Indian Institute of Technology, Bombay, India, in 2007.

He is currently an Associate Professor with the National Institute of Technology (NITRR), Raipur, India. Before joining NITRR, he was with NIT-Warangal, as an Associate Professor, and the Solar Energy Business Group of Schneider Electric, as a Senior Design Engineer, with the R&D Department, Bangalore, India. His research interests include power electronics applications in nonconventional energy conditioning, power quality, and distributed generation.

Sumon Dhara (Student Member, IEEE) received the B.Tech degree in electrical engineering from the Kalyani Government Engineering College, Kalyani, India, in 2014, and the M.Tech degree in 2016 from the National Institute of Technology Warangal, Warangal, India, where he is currently working toward the Ph.D. degree.

He was an Senior Research Fellow under the DST-SERI funded project "Optimized and Efficient Stand-Alone PV System for Rural Applications." His research interests include the advanced PWM schemes and multilevel inverter configurations for renewable energy-based systems.

Vivek Agarwal (Fellow, IEEE) received the B.Sc. degree (Hons.) in physics from St. Stephen's College, Delhi University, Delhi, India, in 1985, the M.E. degree in electrical engineering from the Indian Institute of Science, Bangalore, India, in 1990, and the Ph.D. degree in electrical engineering from the University of Victoria, Victoria, BC, Canada, in 1994.

After a brief stint with Statpower Technologies, Burnaby, BC, Canada, as a Research Engineer, during 1994–1995, he was with the Department of Electrical Engineering, Indian Institute of Technology–Bombay, Mumbai, India, where he is currently a Professor. His research interests include power electronics with focus on power quality issues, renewable energy conditioning, and microgrids.

Dr. Agarwal serves on the editorial boards of the IEEE TRANSACTIONS ON POWER ELECTRONICS and the IEEE TRANSACTIONS ON INDUSTRY APPLICATIONS. He was also Editor-in-Chief for IEEE TRANSACTIONS ON SMART GRID. He is also a Fellow of the Indian National Academy of Engineering and the Institution of Electronics and Telecommunication Engineers.